Antarctic sea ice variability during 1958–1999: A simulation with a global ice-ocean model

Thierry Fichefet, Benoît Tartinville, and Hugues Goosse

Institut d'Astronomie et de Géophysique Georges Lemaître, Université Catholique de Louvain, Louvain-la-Neuve, Belgium

Received 17 September 2001; revised 5 March 2002; accepted 24 January 2003; published 29 March 2003.

[1] A hindcast simulation is carried out with a global ice-ocean model driven by the National Centers for Environmental Prediction (NCEP)–National Center for Atmospheric Research (NCAR) reanalysis daily surface air temperatures and winds in order to document the variability of the Antarctic sea ice cover during 1958–1999. The model consists of an ocean general circulation model coupled to a thermodynamic-dynamic sea ice model with viscous-plastic rheology. Its horizontal resolution is of 1.5° × 1.5°. Both the mean state and variability of the Antarctic ice pack over the satellite observing period are reasonably well reproduced by the model. In particular, from November 1978 to September 1998, the model produces an overall increasing trend in ice area (defined as the total area of ice-covered ocean) of 11,400 ± 2300 km^2 yr^{-1}, which falls within the range of current uncertainty. The model annual mean, area-averaged ice thickness displays no significant trend over 1958–1999. In contrast, a retreat of the pack is simulated during the second half of the 1970s and the beginning of the 1980s, leading to a loss of ice cover of roughly 0.5 × 10^6 km^2 between 1958–1976 and 1982–1999. The marked weakening of the Antarctic semiannual oscillation that occurred since the mid-to-late 1970s seems to be partially responsible for this behavior. Part of the modeled decline might however be spurious and due to the 1979 change in the observing systems utilized in the NCEP–NCAR reanalysis. The simulation also reveals a pronounced decadal variability (8–10 years) in both ice area and thickness. Locally, the changes in ice thickness can reach 1 m during a particular cycle. *INDEX TERMS:* 4207 Oceanography: General: Arctic and Antarctic oceanography; 4215 Oceanography: General: Climate and interannual variability (3309); 4255 Oceanography: General: Numerical modeling; 4540 Oceanography: Physical: Ice mechanics and air/sea/ice exchange processes; *KEYWORDS:* Antarctic sea ice variability, global sea ice-ocean model, sea ice extent, drift and thickness, Southern Ocean

Citation: Fichefet, T., B. Tartinville, and H. Goosse, Antarctic sea ice variability during 1958–1999: A simulation with a global ice-ocean model, *J. Geophys. Res.*, *108*(C3), 3102, doi:10.1029/2001JC001148, 2003.

1. Introduction

[2] At the southern high latitudes, the presence of sea ice significantly affects the interactions between atmosphere and ocean. Due to its high albedo and low thermal conductivity, sea ice alters the radiative and turbulent components of the surface heat balance, cutting the absorption of shortwave radiation down to less than 20% in the case of snow covered ice and reducing the turbulent heat fluxes by 1 to 2 orders of magnitude in winter. In addition, sea ice intercepts most of the snow falling during the cold season, thus preventing it from immediately contributing to the ocean freshwater balance. Finally, the ice pack hinders the free exchange of momentum between atmosphere and ocean. Another facet of the influence of sea ice upon the Antarctic climate is related to the fact that it reshapes the seasonal cycle of the atmospheric and oceanic fields. In the first place, the release and absorption of latent heat that respectively accompany the growth and decay phases of the ice cover tend to delay the seasonal surface temperature extremes. In the second place, the influx of salt into the ocean during ice formation and the freshwater input during ice melting tend to alter the density structure of the upper ocean and hence the ocean thermohaline circulation. These effects, together with the vast expanse of the Antarctic sea ice cover during wintertime (∼19 × 10^6 km^2 in September), ensure the importance of sea ice in the Antarctic climate system. Major changes in Antarctic climate will inevitably involve changes in the sea ice cover, so that monitoring, modeling, and seeking to understand the ice variability on seasonal, interannual, and longer timescales are fundamental aspects of seeking to understand polar climate and polar climate change.

[3] The large-scale variability of the Antarctic sea ice coverage can be studied at up to decadal timescales using existing satellite data sets. Microwave-derived time series of ice concentration (the percentage of ice-covered ocean) are now among the longest continuous satellite-derived geophysical records, extending over more than 20 years [*World*

0148-0227/03/2001JC001148$09.00

Climate Research Programme, 2001]. The scanning multichannel microwave radiometer (SMMR) on board the Nimbus 7 satellite provided data from 1978 to 1987 [*Gloersen et al.*, 1992], and the special sensor microwave imagers (SSMIs) on board the Defense Meteorological Satellite Programme F8, F11, and F13 satellites have provided data since 1987 [e.g., *Gloersen et al.*, 1999]. By intercalibrating the different sensors during the overlap periods, *Cavalieri et al.* [1997] obtained uniform estimates of Antarctic sea ice extent (defined as the area within the ice-ocean margin limited by the 15% concentration contour) and area from November 1978 to December 1996. Their data reveal pronounced seasonal and interannual variabilities, with an overall increasing trend of $14{,}300 \pm 2600$ km^2 yr^{-1} ($13{,}800 \pm 2500$ km^2 yr^{-1}) in ice extent (area) over the 18.2-year period. According to *Watkins and Simmonds* [2000], this slight upward trend is largely attributable to an increase in ice extent (area) during the mid-1990s. A study similar to that of *Cavalieri et al.* [1997] was conducted by *Bjørgo et al.* [1997]. These authors, who employed a different algorithm to retrieve the ice concentrations from the satellite measurements, concluded there has been no statistically significant change in Antarctic sea ice extent and area during the period November 1978 through August 1995.

[4] Much less is known on the variability of the Antarctic sea ice areal coverage in the more distant past. *Chapman and Walsh* [1993], using a record extending from 1973 to 1990 based on the weekly U.S. Navy–National Oceanic and Atmospheric Administration (NOAA) National Ice Center charts (compiled from high-resolution satellite imagery, aircraft and ship reports, but also including passive microwave data when necessary), found no statistically significant trend in ice extent for the 18-year period as a whole. Nonetheless, they noticed some low-frequency modulation, with maxima in the early 1970s and early 1980s and minima in the late 1970s and late 1980s. The greatest ice extents were reached in 1973–1975. More recently, *de la Mare* [1997] inferred from whaling records that the Antarctic summer sea ice edge has moved southward by 2.8° of latitude between the mid-1950s and the early 1970s. This suggests a decline in the area covered by sea ice of some 25%. The indirect nature of his reconstruction, however, introduces substantial uncertainty into this conclusion.

[5] Another important variable of state of the sea ice pack is its thickness. Although innovative methods to estimate spatially averaged sea ice thickness utilizing spaceborne altimetry appear promising [e.g., *Giles and Laxon*, 2001], the ice thickness is still best measured by detecting the ice draft from below by use of upward looking sonars (ULSs) in moorings or on submarines, by airborne laser profiling, by employing airborne electromagnetic techniques, or by drilling [*Wadhams*, 1994]. Unfortunately, there have been so far very few systematic measurements of ice thickness in the Antarctic, and the available time series are rather short [e.g., *Strass and Fahrbach*, 1998; *Harms et al.*, 2001]. As a consequence, there is little information on the variability of the pack thickness. Actually, even the broad spatial and seasonal climatology of ice thickness is not well known.

[6] In the present work, a global ice-ocean model designed for climate studies is used to document the variability of the Antarctic sea ice during the 42-year period 1958–1999. Daily data of surface air temperature and wind are utilized to produce the year-to-year variations of the ice cover. We focus on analyzing the variability of the pack area and thickness. A validation of the model is also performed by comparing results from the last 2 decades of this hindcast simulation with the available observational data. Experiments of this type have been recently carried out by *Beckmann and Timmermann* [2001] and *Timmermann et al.* [2002a, 2002b] with a regional model of the Southern Ocean and of its sea ice. However, the authors limited their analysis to the Weddell Sea sector and concentrated on the variability of dense water production.

2. The Model, Forcing, and Experimental Design

[7] The model used here is based on that of *Goosse and Fichefet* [1999]. It is made up of a global ocean general circulation model (OGCM) coupled to a comprehensive thermodynamic-dynamic sea ice model. The OGCM is a primitive equation, free surface model that rests on the usual set of assumptions, i.e., the hydrostatic equilibrium and the Boussinesq approximation [*Deleersnijder and Campin*, 1995; *Campin and Goosse*, 1999]. It contains a sophisticated formulation of the subgrid-scale vertical mixing derived from the *Mellor and Yamada* [1982] level-2.5 turbulence closure scheme [*Goosse et al.*, 1999] and a parameterization of density-driven downslope flows [*Campin and Goosse*, 1999]. The current version also includes the *Gent and McWilliams* [1990] parameterization of the tracer transport due to mesoscale eddies and a physically based representation of the upper boundary condition for the salinity balance [*Tartinville et al.*, 2001]. Apart from a reduction of the snow thermal conductivity from 0.31 to 0.22 W m^{-1} K^{-1} (see *Fichefet et al.* [2000] for justification), the sea ice model is identical to that of *Fichefet and Morales Maqueda* [1997, 1999]. Sensible heat storage and vertical heat conduction within snow and ice are determined by a three-layer model (one layer for snow and two layers for ice). The effect of the subgrid-scale snow and ice thickness distributions is accounted for through effective thermal conductivities, which are computed by assuming that the snow and ice thicknesses are uniformly distributed between zero and twice their mean value over the ice-covered portion of the grid cell. The storage of latent heat inside the ice resulting from the trapping of shortwave radiation by brine pockets is taken into account. The model also allows for the presence of leads within the ice pack. Vertical and lateral growth/decay rates of the ice are obtained from prognostic energy budgets at both the bottom and surface boundaries of the snow-ice cover and in leads. When the load of snow is large enough to depress the snow-ice interface under the water level, seawater is supposed to infiltrate the entirety of the submerged snow and to freeze there, forming a snow ice cap. For the momentum balance, sea ice is considered as a two-dimensional continuum in dynamical interaction with atmosphere and ocean. The viscous-plastic constitutive law proposed by *Hibler* [1979] is used for calculating the internal ice force. The physical fields that are advected are the ice concentration, the snow volume per unit area, the ice volume per unit area, the snow enthalpy per unit area, the ice enthalpy per unit area, and the brine reservoir per unit area. The coupled model has a

horizontal resolution of 1.5° × 1.5°, and there are 30 unequally spaced vertical levels in the ocean. The bathymetry is a discretized version of the real World Ocean bottom topography.

[8] Daily surface air temperatures and winds from the NCEP–NCAR reanalysis project for the period 1948–1999 [*Kalnay et al.*, 1996] are utilized to drive the model. The other atmospheric input fields consist of climatological monthly surface relative humidities [*Trenberth et al.*, 1989], cloud fractions [*Berliand and Strokina*, 1980], and precipitation rates [*Xie and Arkin*, 1996]. The surface fluxes of heat are determined from these data by using empirical parameterizations described by *Goosse* [1997]. Evaporation/sublimation is derived from the turbulent flux of latent heat. The freshwater inflows from the largest rivers are prescribed according to the monthly climatology of *Grabs et al.* [1996]. For the smaller rivers, the annual runoff values of *Baumgartner and Reichel* [1975] are employed. In addition, a relaxation toward observed annual mean salinities [*Levitus*, 1982] is applied in the 10-m-thick surface grid box with a time constant of 2 months. This weak restoring circumvents the surface salinity drift that would occur through the lack of any stabilizing feedback if the model is forced with slightly incorrect evaporation, precipitation, and runoff fields. The momentum fluxes at the various interfaces are obtained from standard bulk formulas. The parameterization of *Large and Pond* [1981] is utilized to compute the drag coefficient between air and water. For the drag coefficients between air and snow/ice and between ice and water, we use constant values of 2.25×10^{-3} and 5×10^{-3}, respectively. This leads to a ratio of these two coefficients of 0.45, which is consistent with values adopted in other modeling studies of the Antarctic sea ice [e.g., *Stössel*, 1992; *Fischer and Lemke*, 1994; *Harder and Fischer*, 1999]. The ice strength parameter P* is set equal to 3×10^4 N m^{-2}, a classical value for a daily varying wind-forcing [e.g., *Hibler and Ackley*, 1983].

[9] The hindcast simulation covered the period 1948–1999 and started from a quasi-equilibrium state obtained under a monthly climatological forcing built from the above-mentioned data fields. The first 10 years of the experiment are excluded from the analysis that follows because the ice characteristics during this period were significantly affected by the initial fields and because of the poor quality of the NCEP–NCAR reanalysis data during this time interval [*Hines et al.*, 2000; *Kistler et al.*, 2001]. The reader is referred to *Tartinville et al.* [2002] for a discussion of the simulation results related to the Arctic ice cover. Here, we only report on the Antarctic sea ice results.

[10] When interpreting the simulation results, one has to bear in mind that the model is forced with surface air temperatures and winds that reflect the specification of sea ice in the spectral T62 atmospheric general circulation model used to produce the NCEP–NCAR reanalysis. For the period extending from 1948 to 1971, the reanalysis system utilized climatological monthly sea ice covers in the Southern Hemisphere. For the years 1972–1978, monthly sea ice extents from the United Kingdom Met Office global ice and sea surface temperature data set were employed. Finally, for 1979 and beyond, daily sea ice covers based on the SMMR–SSMI data were used (R. Grumbine and R. Kistler, personal communication, 2002). In all cases, a value of 1 or 0 was assigned to the ice concentration.

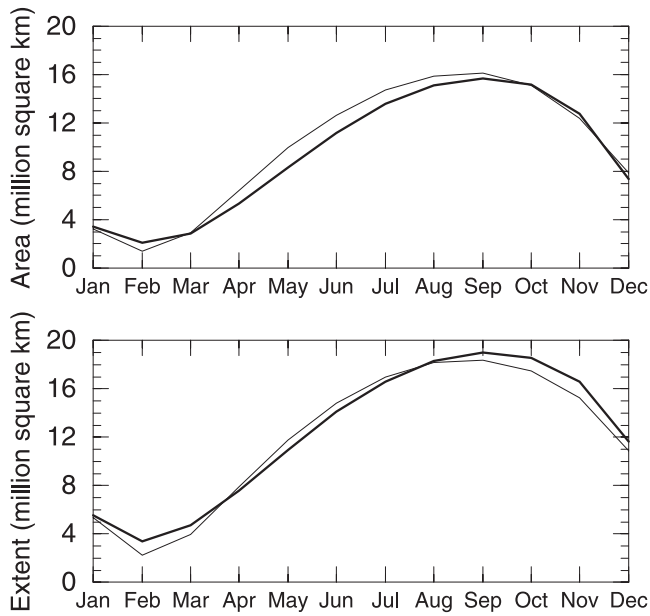

Figure 1. Average seasonal cycles of sea ice (top) area and (bottom) extent over the period November 1978 through September 1998 as simulated by the model (thin curves) and as observed (thick curves).

3. Results

3.1. Comparison With Observational Data

[11] In this subsection, we compare the model outputs with data collected during the SMMR-SSMI years. Figure 1 displays the computed and observed mean seasonal cycles of Antarctic sea ice area and extent for the period November 1978–September 1998. The observed cycles have been constructed from the Bootstrap sea ice concentrations derived from the SMMR and SSMI measurements [*National Snow and Ice Data Center*, 1999]. It can be seen that the model does fairly well in simulating the timing of the maximum and minimum areal coverages of ice. Both the modeled and observed ice areas and extents reach their minimum in February and culminate in September. Compared to this particular data set, the model pack as a whole seems slightly too compact throughout the year and exhibits too rapid a retreat in early spring and midsummer. As a consequence, the simulated ice area is lower than observed by 0.7×10^6 km^2 in February and higher than observed by 0.4×10^6 km^2 in September. Note that the largest discrepancy occurs in fall, where the model overestimates the ice area by 1.7×10^6 km^2. Regarding the ice extent, it appears 0.6×10^6 km^2 too low both in February and September. Reasonably enough, we can put into question the ability of the model to correctly represent the intricate thermodynamics and dynamics of real leads. However, part of the discrepancy has also its origin in inaccuracies in the model forcing. Furthermore, one should mention that there are substantial differences in the satellite-derived sea ice concentrations depending on which algorithm is utilized to retrieve the ice compactness from the passive microwave

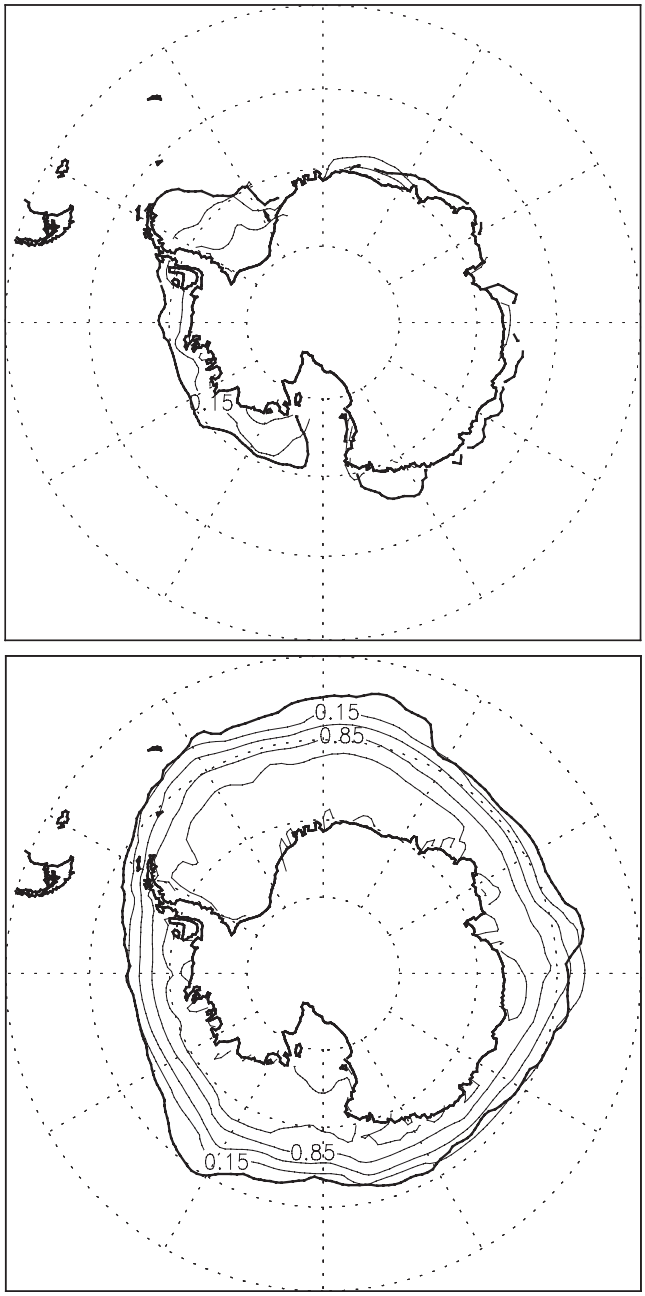

Figure 2. Average (top) February and (bottom) September sea ice concentrations over the years 1979–1998 as computed by the model. Selected contours are 0.15, 0.50, 0.85, and 0.95. Also shown are the observed 0.15 ice concentration contours (thick lines).

data [e.g., *Steffen et al.*, 1992; *Comiso et al.*, 1997; *Markus and Cavalieri*, 2000]. So, the model might actually do a better job than the comparison with the Bootstrap data suggests.

[12] Figure 2 depicts the average February and September sea ice concentrations over the years 1979–1998 as calculated by the model. In February, the main shortcomings of the simulation are too low ice concentrations in the southwestern Weddell Sea and a lack of ice near the tip of the Antarctic Peninsula. At least two factors contribute to these erroneous features: (1) the fierce southwesterly winds that blow during winter and early spring off the east coast of the peninsula south of 70°S in the NCEP–NCAR reanalysis and that carry away the ice, and (2) a warm bias in the NCEP–NCAR surface air temperatures north of this area (which is probably due to the crude representation of the tip of the Antarctic Peninsula in the model used for the reanalysis [*Windmüller*, 1997]). One also notices that the modeled ice margin is somewhat south of the observed one in the western Pacific Ocean sector and in the Amundsen and Bellingshausen Seas. In September, the simulated location of the ice edge is generally in excellent agreement with the observed one. Nonetheless, the model ice cover does not protrude sufficiently far northward in the eastern Weddell Sea and in the eastern Ross Sea.

[13] Contrary to early investigations of Antarctic sea ice with global ice-ocean models [e.g., *Legutke et al.*, 1997; *Stössel et al.*, 1998; *Goosse and Fichefet*, 1999], our model does not produce excessive sea ice melting associated with too intense an open ocean convection in the Southern Ocean. This is due to a combination of several factors. First, the sophisticated parameterization of the subgrid-scale vertical mixing used here allows a better simulation of the mixed layer depth and thus of heat exchanges between ocean and ice in the Southern Ocean [*Goosse et al.*, 1999]. Second, the current version of our model includes the *Gent and McWilliams* [1990] parameterization of the tracer transport due to mesoscale eddies, which is known to reduce open ocean convection in the Southern Ocean and hence to contribute in maintaining sea ice there [e.g., *Danabasoglu and McWilliams*, 1995; *Hirst and McDougall*, 1996; *England and Hirst*, 1997; *Goosse et al.*, 2001]. Third, the model sea surface salinity is relaxed toward observed annual mean values everywhere. This restoring generally adds fresh water into the high latitude Southern Ocean, which tends to stabilize the water column [*Goosse and Fichefet*, 1999; *Marsland and Wolff*, 2001]. Finally, although still rather coarse, the model resolution is enhanced compared to previous studies, and this affects positively the results in the Southern Ocean.

[14] The modeled and observed time series of monthly sea ice area and extent anomalies over the time interval November 1978 through September 1998 are illustrated in Figure 3. The anomalies were obtained by taking the monthly value for each individual month and by subtracting the average value for that month over the 19.9-year period. Here again, the observed values were derived from the Bootstrap ice concentrations. The marked interannual variability seen in the data is well captured by the model. In particular, thanks to the forcing, the model is capable of reproducing the abnormally low ice areal coverage observed during the second half of 1979 and the first half of 1980 as well as the strong positive and negative anomalies in maximum ice area and extent recorded in 1985 and 1986, respectively. The correlation coefficient between the simulated and observed time series amounts to 0.67 for the ice area and 0.55 for the ice extent. On the other hand, the standard deviation of the modeled anomalies is 0.41×10^6 km^2 for the ice area and 0.49×10^6 km^2 for the ice extent. These values are consistent with the observed ones (0.34×10^6 km^2 and 0.40×10^6 km^2, respectively), although a bit overestimated. A least squares regression analysis of the

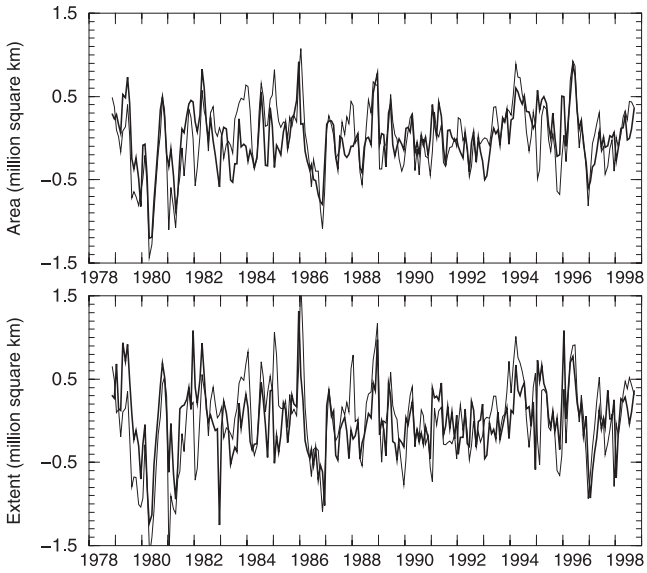

Figure 3. Simulated (thin curves) and observed (thick curves) monthly sea ice (top) area and (bottom) extent anomalies over the period November 1978 through September 1998.

model results reveals a slight increase of 11,400 ± 2300 km^2 yr^{-1} in ice area and 13,800 ± 2700 km^2 yr^{-1} in ice extent during the 19.9-year period. As for the Bootstrap data, they show an overall increasing trend of 10,500 ± 1900 km^2 yr^{-1} in ice area but no statistically significant trend in ice extent. Note that these observational estimates somewhat differ from those of *Bjørgo et al.* [1997] and *Cavalieri et al.* [1997]. Two main reasons may be invoked to explain this discrepancy. First, we have included the recent data in the observed anomaly time series. Since these series are relatively brief, even a single unusual year can substantially affect the estimated trend [*Bjørgo et al.*, 1997]. Second, the ice concentration data used in the two above-mentioned studies were derived from different passive microwave algorithms.

[15] Figure 4 shows the average September ice velocities over 1987–1997 computed by the model and reconstructed from animations of SSMI brightness temperatures [*Drinkwater and Liu*, 1999]. The accuracy of the observational data is discussed by *Maslanik et al.* [1998]. The Antarctic Circumpolar Drift, a cyclonic circulation that transports ice from west to east all around Antarctica, and the East Wind Drift, an easterly coastal flow that also circumscribes the continent, are both well reproduced by the model. The model also simulates a pronounced Weddell Gyre, a cyclonic ice circulation in the eastern Ross Sea, and strong offshore ice drifts in the western Ross Sea and in the vicinity of the Amery Ice Shelf, all features that are present in the observations. The magnitudes of the modeled ice velocities compare reasonably well with the observed ones in the 30°E–75°E sector and in the Amundsen and Bellingshausen Seas, but appear too high elsewhere. A fine tuning of the drag coefficients and to a lesser extent of the ice strength parameter, whose values are rather uncertain, should allow to reduce this bias [e.g., *Harder and Fischer*, 1999]. Part of the discordance also results from inaccuracies in the wind-forcing. This is the case, for instance, in the southwestern Weddell Sea, where abnormally strong southwesterly winds (see above) lead to too intense a northward ice drift.

[16] The geographical distribution of the model ice thickness is largely determined by the ice drift patterns. In particular, convergent ice motions yield ice buildups of up to 2 m in thickness, on average, in the southern Weddell Sea and in the southeastern Ross Sea during the cold season (Figure 5). The simulated ice thicknesses off East Antarctica and in the Ross, Amundsen, and Bellingshausen Seas are

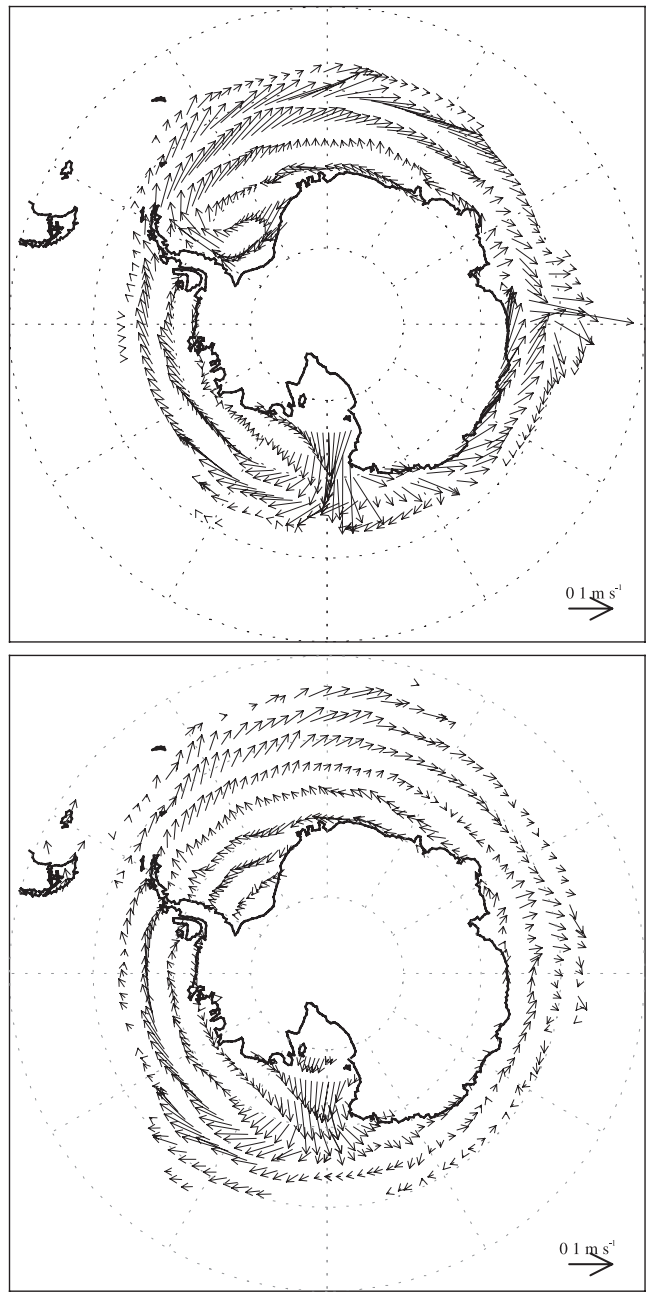

Figure 4. Average September sea ice velocities over the years 1987–1997 (top) as simulated by the model and (bottom) as observed. The scale vector corresponds to an ice velocity of 1 m s^{-1}.

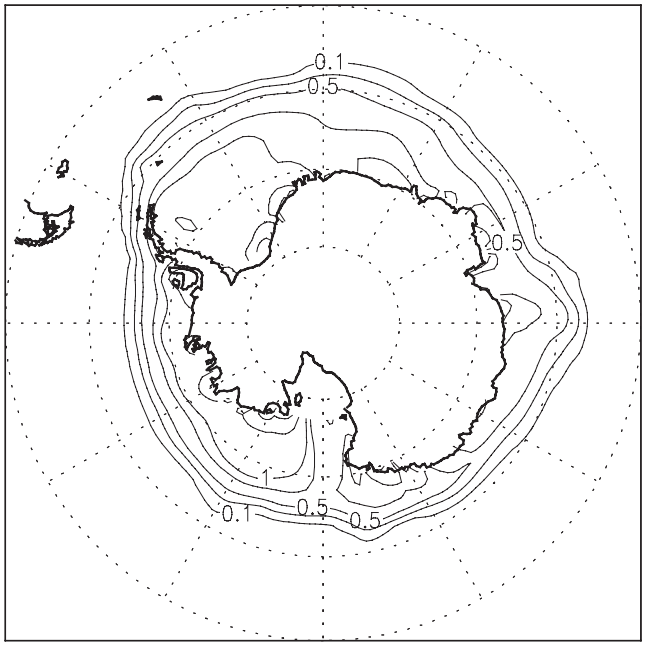

Figure 5. Average September sea ice thicknesses over the years 1958–1999 as computed by the model. Selected contours are 0.1, 0.3, 0.5, 0.8, 1.0, 1.5, and 2 m.

within the range hitherto reported from drillings and ship-based observations [e.g., *Allison et al.*, 1993; *Jeffries et al.*, 1994; *Worby et al.*, 1996, 1998; *Jeffries and Adolphs*, 1997; *Adolphs*, 1998].

[17] Between 1990 and 1996, several ULSs were deployed in the Weddell Sea on two transects extending from the tip of the Antarctic Peninsula to Kapp Norvegia and from the Antarctic continent northward along the Greenwich meridian [*Strass and Fahrbach*, 1998; *Harms et al.*, 2001]. In Figure 6, we compare the ice thicknesses computed by the model in the grid cells containing the mooring sites with those derived from the ULS measurements. At moorings 208, 209, 210, 227, 229, and 231 (see Figure 6 for mooring locations), the agreement between the simulation and observations is quite good. By contrast, the model significantly underestimates the ice thickness at moorings 207 and 217. This error is mostly caused by the warm bias in surface air temperature in this area (see above), which prevents the survival of multiyear ice. In addition, we must point out that the ULS-derived ice thicknesses in this sector are notably higher than estimates obtained by drilling. For instance, *Lange and Eicken* [1991] reported a mean ice thickness of only 1.3 m in the northwestern Weddell Sea close to ULS moorings 207 and 217. Reasons for this difference between data are unclear [*Strass and Fahrbach*, 1998]. The simulated ice cap also appears too thin at the near-coast moorings 212, 231, and 232. Furthermore, the model fails in reproducing the pronounced variability observed at mooring 212. According to *Harms et al.* [2001], prevailing easterly winds off Kapp Norvegia have a slight offshore component. As a consequence, coastal leads and polynyas develop, in which new ice can be continuously produced. When easterly winds weaken, or even reverse, the combined effect of winds and currents with the presence of the coast leads to the formation of pressure ridges there. Relevant scales for this process are much smaller than the model grid size, so that the variability recorded by the ULS can hardly be simulated by the model.

[18] Although we have identified a certain number of discrepancies over the satellite observing era between the results of our hindcast simulation and observational data, the discussion above demonstrates that the model shows acceptably good agreement with enough aspects of the real behavior of the Antarctic sea ice to permit a sound study of the variability of the ice pack during the period 1958–1999.

3.2. Analysis of the Sea Ice Variability During 1958–1999

[19] The upper panel of Figure 7 depicts the monthly sea ice area anomalies produced by the model over 1958–1999. As in Figure 3, the anomalies are relative to November 1978 through September 1998. The most striking feature is the marked decline in ice area taking place during the second half of the 1970s and the beginning of the 1980s. Between 1958–1976 and 1982–1999, the model pack undergoes a retreat of 0.48×10^6 km^2, on average. In order to evaluate the influence of the temperature forcing on this behavior, we run a sensitivity experiment including interannual and longer-term variability of the wind field only. In this case, a decrease in ice area still occurs (see lower panel of Figure 7), but its magnitude is reduced to 0.28×10^6 km^2. This result suggests that both the temperature and wind-forcings contribute significantly to the loss of ice cover observed in the control simulation. Figure 8 shows the differences in average ice concentration for September between the two time intervals 1982–1999 and 1958–1976 of the control experiment. Decreases in ice compactness greater than 0.2 are visible near the ice margin in the western Weddell Sea, off Princess Ragnhild Coast, between 90°E and 180°E, and in the Amundsen and Bellingshausen Seas. In contrast, the region off Mawson Coast and the Amery Ice Shelf experiences an increase in ice concentration of up to 0.3.

[20] The abrupt shrinkage of the ice pack simulated by the model happens later and is much weaker than the one deduced by *de la Mare* [1997] from the analysis of whaling records (see section 1). One cannot rule out the possibility that the modeled decline be due, at least partly, to a change in the observing systems utilized in the NCEP–NCAR reanalysis. Actually, such a change took place in 1979 when the global operational use of satellite soundings was introduced [*Kistler et al.*, 2001]. However, it is noteworthy that the computed monthly anomalies in sea ice area compare favorably with the observed ones during the last two months of 1978 (see upper panel of Figure 3). Furthermore, there is some observational evidence that the ice cover was more extensive in the mid-1970s than during recent decades [e.g., *Weatherly et al.*, 1991; *Chapman and Walsh*, 1993; *Folland et al.*, 2001].

[21] A possible explanation for the retreat of the ice pack might be the rather dramatic weakening of the semiannual oscillation (SAO) that occurred since the mid-to-late 1970s. The SAO is observed throughout the depth of the troposphere at middle and high latitudes of the Southern Hemisphere. At the surface, it is characterized by an expansion and weakening of the circumpolar trough of low pressure surrounding Antarctica from March to June and September to December, and by a contraction and intensification from

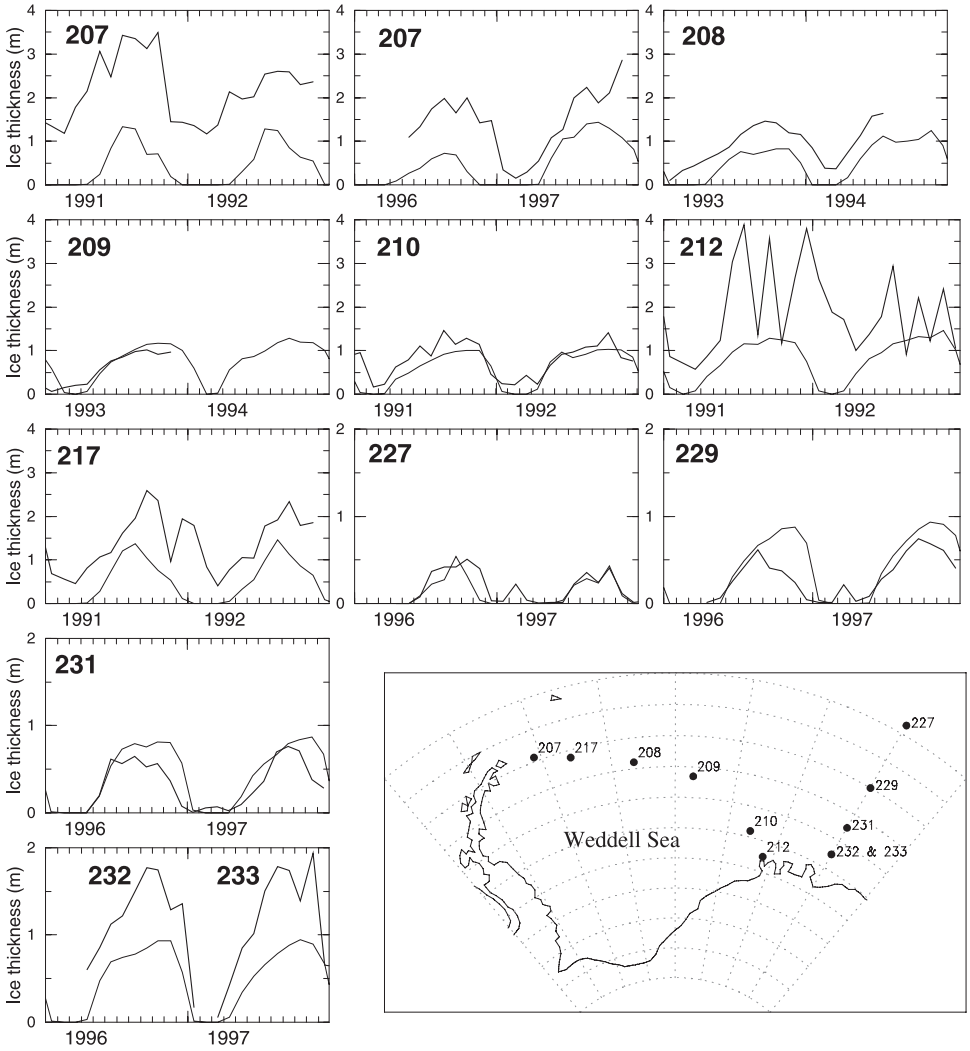

Figure 6. Simulated (thin curves) and observed (thick curves) time series of monthly mean sea ice thickness at several ULS mooring sites in the Weddell Sea. The mooring locations are shown in the bottom right panel.

June to September and December to March. This half-yearly wave in sea level pressure arises from differences in heat uptake between the Antarctic continent and its oceanic surroundings [*van Loon*, 1967; *Meehl*, 1991]. It is well known that the SAO plays a key role in controlling the Antarctic sea ice areal coverage. In particular, *Harangozo* [1997] and *Van den Broeke* [2000a] have shown that during years with a weak SAO, there is an appreciable decrease of wintertime ice cover in the Amundsen and Bellingshausen Seas associated with enhanced northerly circulation (advection of warm air) and stronger westerlies (enhanced mechanical break-up of sea ice). This rule seems also to apply to the western Weddell Sea, the western Pacific Ocean sector, and the western Ross Sea [*Van den Broeke*, 2000b, 2000c]. A number of observational studies have revealed that the amplitude of the SAO decreased considerably after the mid-to-late 1970s [e.g., *van Loon et al.*, 1993; *Hurrell and van Loon*, 1994; *Meehl et al.*, 1998, *Van den Broecke*, 1998, 2000b]. According to *Van den Broecke* [1998, 2000b], who analyzed the longest records of surface pressure available, this change might be part of the long-term natural variability of the SAO. Figure 9 displays the

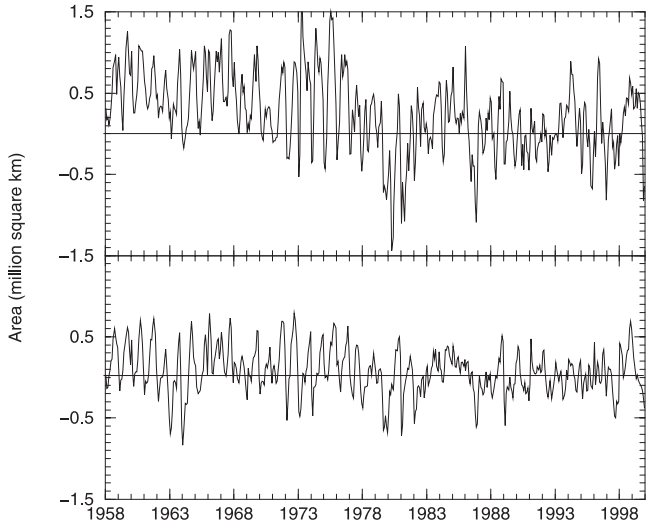

Figure 7. Monthly sea ice area anomalies over 1958–1999 from (top) the control simulation and (bottom) the sensitivity experiment with no year-to-year variation in surface air temperature.

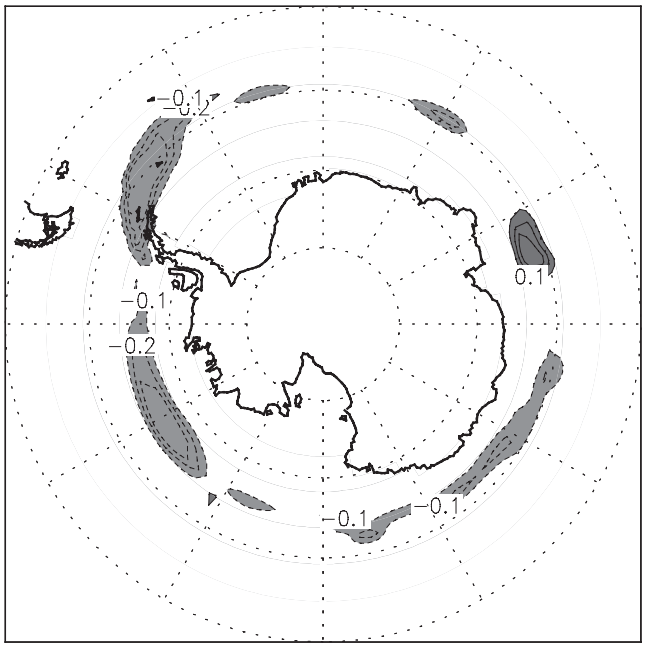

Figure 8. Differences in average sea ice concentration for September between the two time intervals 1982–1999 and 1958–1976 of the control simulation. The contour interval is 0.1. Dark (light) shading denotes values greater (lower) than 0.1 (−0.1).

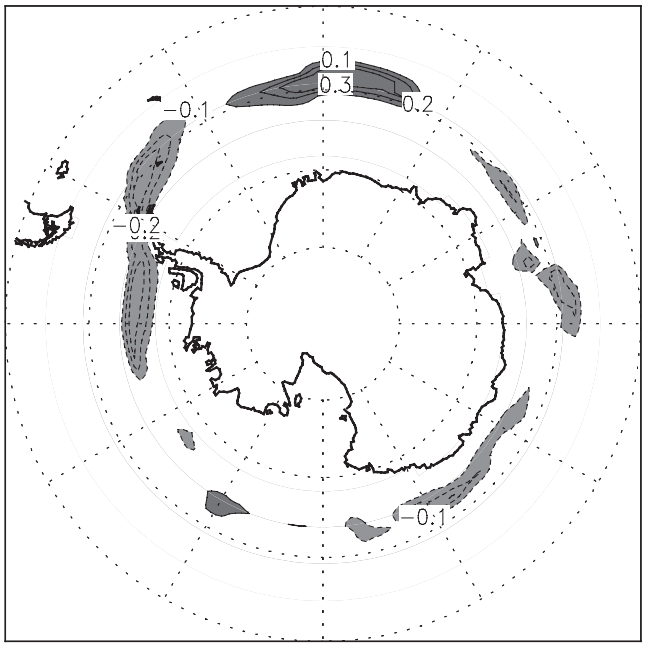

Figure 9. Differences in average sea ice concentration at the time of the maximum ice extent between years with a weak SAO (1968, 1969, 1981, 1985, 1989, 1993, and 1998) and years with a strong SAO (1964, 1974, 1975, 1976, 1977, 1982, and 1990) as simulated in the control run. The years were chosen by applying the criterion proposed by *Van den Broeke* [2000b]. The contour interval is 0.1. Dark (light) shading denotes values greater (lower) than 0.1 (−0.1).

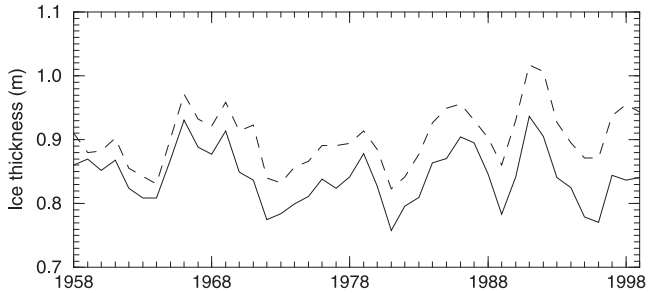

Figure 10. Time series between 1958 and 1999 of annual mean, area-averaged sea ice thickness from the control simulation (solid curve) and the sensitivity experiment with no year-to-year variation in surface air temperature (dashed curve).

modeled differences in average ice concentration at the time of the maximum ice extent between years with a weak SAO and years with a strong SAO in the NCEP–NCAR reanalysis data set. There is a degree of resemblance between this figure and Figure 8. This similarity suggests that the weaker SAO conditions from the second half of the 1970s onward are partially responsible for the shrinkage of the ice pack noticed in our simulation.

[22] The upper panel of Figure 7 shows that, in addition to the abrupt decrease discussed above, the ice area exhibits a decadal variability. This is confirmed by a spectral analysis, which reveals a significant peak at periods of 8–10 years. These decadal fluctuations are also present in the sensitivity experiment using a climatological thermal forcing, with a reduced amplitude (see lower panel of Figure 7). The largest winter ice areas ($\sim 17.5 \times 10^6$ km^2) are reached in 1959, 1967, and 1975. It is worth mentioning that the model fails in simulating the Weddell Polynya, this opening of $0.1–0.3 \times 10^6$ km^2 in the sea ice cover that was observed to develop in the Weddell Sea in each of the years 1974–1976 [e.g., *Zwally et al.*, 1983]. This is not surprising since this feature seems to involve, at least partly, oceanic processes that cannot be resolved by our coarse-resolution ice-ocean model [e.g., *Beckmann et al.*, 2001; *Holland*, 2001].

[23] Complementary information on the variability of the pack is provided by the temporal evolution of the annual mean, area-averaged ice thickness (Figure 10). In order to separate as much as possible the thickness signal from the area signal, this quantity was defined as the annual mean total ice volume divided by the annual mean ice area. Unlike the ice area, it exhibits no noticeable trend over the period 1958–1999. A decadal variability is however apparent. The peak-to-trough changes amount to 0.10–0.15 m, which corresponds to 12–18% of the long-term mean ice thickness. This variability is almost entirely caused by the wind-forcing. Indeed, the sensitivity experiment with no year-to-year variation in surface air temperature shows fluctuations that are nearly identical to those of the control simulation (see Figure 10). Regionally, the modifications in ice thickness can be substantial during a particular cycle. This can be seen from Figure 11, which gives the geographical distribution of the change in September ice thickness from 1986 to 1989 as simulated in the control case. Decreases in ice thickness of 0.5–1 m occur in the north-

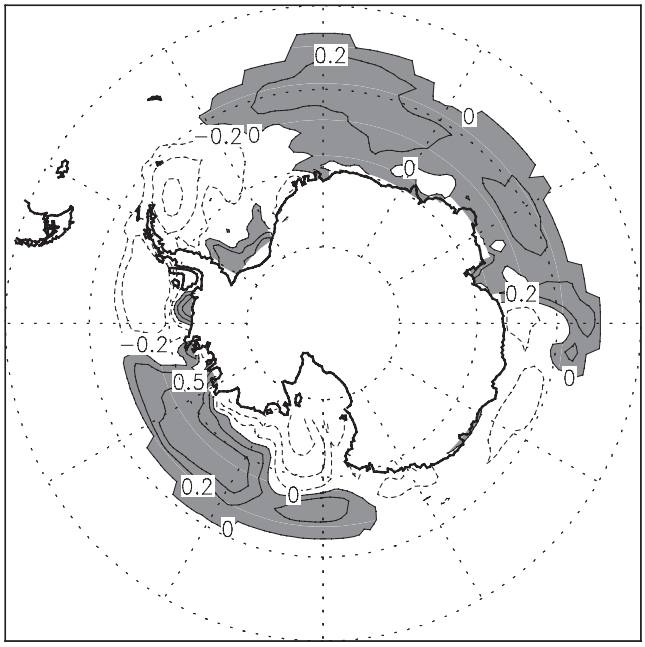

Figure 11. Changes in September sea ice thickness from 1986 to 1989 as simulated in the control run. Selected contours are −1.0, −0.5, −0.2, 0.0, 0.2, 0.5, and 1.0 m. Positive values are shaded.

western Weddell Sea, in the northern Bellingshausen Sea, and in the southern Ross Sea. Conversely, the ice gets thicker by more than 0.5 m in the coastal regions of the southern Weddell and Bellingshausen Seas, in the Amundsen Sea, and in the northeastern Ross Sea. The anomalies are found to propagate eastward, taking 8 years on average to encircle Antarctica.

4. Discussion and Conclusion

[24] A hindcast simulation has been conducted with a global, coarse-resolution ice-ocean model forced with the NCEP–NCAR reanalysis daily surface air temperatures and winds in order to document the variability of the Antarctic sea ice cover over the period 1958–1999. We stress that this simulation did not include the potential contribution from the hydrological cycle variability to the changes of sea ice on interannual or longer timescales.

[25] The NCEP–NCAR reanalysis data set is the longest global gridded atmospheric data set available today. Unfortunately, it contains a number of errors discovered by internal NCEP monitoring and by outside users. Two of them deserve a particular attention in the context of the present study. First, the Australian Surface Pressure Bogus Data for the Southern Hemisphere for 1979–1992 were read with a 180° error in longitude. This mistake primarily affects the area south of 40°S [*Kistler et al.*, 2001]. Second, artificial long-term surface pressure reductions are apparent south of 45°S [*Hines et al.*, 2000]. These two problems do not seem to impact significantly on our simulation, as both the mean state and variability of the pack over the SMMR–SSMI years are reasonably well reproduced by the model. Several shortcomings were however identified, such as too weak and too thin an ice cover in the western Weddell Sea and too high ice velocities in several sectors of the Southern Ocean. These two particular deficiencies were partly attributed to inaccuracies in the atmospheric forcing fields.

[26] From November 1978 to September 1998, the model sea ice area experiences a slight increase of 11,400 ± 2300 $km^2\ yr^{-1}$, consistent with observational estimates. By contrast, a retreat of the ice pack is simulated during the second half of the 1970s and the beginning of the 1980s, leading to a loss of ice cover of about $0.5 \times 10^6\ km^2$ between 1958–1976 and 1982–1999. Our analysis suggests that the marked weakening of the SAO observed since the mid-to-late 1970s in the real world as well as in the NCEP–NCAR reanalysis contributes to this feature. Part of the simulated decrease in ice area might however be spurious and caused by the introduction in the NCEP–NCAR reanalysis of satellite sounding data in 1979.

[27] No such decline has been detected in the modeled time series of annual mean, area-averaged ice thickness. Actually, this time series exhibits no overall trend over the period 1958–1976. This is an important result, as no information was available prior to our work on the long-term evolution of the pack thickness in the Antarctic.

[28] The simulation also revealed a pronounced decadal variability (8–10 years) in both ice area and thickness. During a particular oscillation, changes in ice thickness of up to 1 m can occur locally. Utilizing data of sea level pressure, surface wind, sea surface temperature, and sea ice edge position, *White and Peterson* [1996] identified a coupled set of wave number-2 climatic anomalies propagating eastward around the Southern Ocean at an average speed of ~8 cm s^{-1}, thus requiring 8–10 years for individual phases of the wave train to circle the globe. They named this propagating phenomenon the Antarctic Circumpolar Wave (ACW). Besides, the strength of the SAO also displays a significant variability at the decadal timescale [e.g., *van Loon et al.*, 1993; *Van den Broecke*, 1998, 2000b]. A natural extension of the present study will be to cross-correlate climate analysis fields with the model outputs in order to explore the possible relationship between these two features and the decadal variability found in our simulation. This variability at both the decadal and multidecadal timescales, if real, will make most difficult the detection of possible trends induced by greenhouse gas warming in the relatively short observational Antarctic ice records available today.

[29] **Acknowledgments.** We wish to thank A. Beckmann, M. R. Drinkwater, M. A. Morales Maqueda, and M. R. Van den Broeke for helpful discussions about various aspects of this work, and we wish to thank the two anonymous referees for their careful reading of the manuscript and constructive criticism. The NCEP–NCAR reanalysis data were provided through the NOAA–CIRES Climate Diagnostics Center, Boulder. The Bootstrap sea ice concentrations, areas, and extents from Nimbus-7 SMMR and DMSP SSMI were obtained from the EOSDIS NSIDC Distributed Active Center (NSIDC DAAC), University of Colorado, Boulder. E. Farhbach kindly supplied the ULS ice draft data used for validating the model. The ice velocity data were provided by courtesy of M. R. Drinkwater and X. Liu from the Jet Propulsion Laboratory, California Institute of Technology, Pasadena, and were processed through a NASA-supported collaborative study with C. Fowler and J. A. Maslanik from the University of Colorado, Boulder. T. Fichefet and H. Goosse are Research Associate and Postdoctoral Researcher at the Belgian National Fund for Scientific Research, respectively. This study was done within the scope of the First and Second Multiannual Scientific Support Plans for a Sustainable Development Policy (Belgian State, Prime Minister's Services, Federal Office for Scientific, Technical, and Cultural Affairs, contracts CG/DD/09A

and EV/10/7D), the concerted research action 097/02-208 (French Community of Belgium, Department of Education, Research, and Formation), the FRFC project 2.4556.99 (Belgian National Fund for Scientific Research), and the French project of operational oceanography MERCATOR. All of this support is gratefully acknowledged.

References

Adolphs, U., Ice thickness variability, isostatic balance and potential for snow ice formation on ice floes in the south polar Pacific Ocean, *J. Geophys. Res.*, *103*, 24,675–24,691, 1998.

Allison, I., R. E. Brandt, and S. G. Warren, East Antarctic sea ice: Albedo, thickness distribution, and snow cover, *J. Geophys. Res.*, *98*, 12,417–12,429, 1993.

Baumgartner, A., and E. Reichel, *The World Water Balance*, 179 pp., Elsevier, New York, 1975.

Beckmann, A., and R. Timmermann, Circumpolar influences on the Weddell Sea: Indication of an Antarctic circumpolar coastal wave, *J. Clim.*, *14*, 3785–3792, 2001.

Beckmann, A., R. Timmermann, A. F. Pereira, and C. Mohn, The effect of flow at Maud Rise on the sea-ice cover-Numerical experiments, *Ocean Dyn.*, *52*, 11–25, 2001.

Berliand, M. E., and T. G. Strokina, *Global Distribution of the Total Amount of Clouds* (in Russian), 71 pp., Hydrometeorological, St. Petersburg, Russia, 1980.

Bjørgo, E., O. M. Johannessen, and M. W. Miles, Analysis of merged SMMR–SSMI time series of Arctic and Antarctic sea ice parameters 1978–1995, *Geophys. Res. Lett.*, *24*, 413–416, 1997.

Campin, J.-M., and H. Goosse, A parameterization of density-driven downsloping flow for a coarse-resolution model in *z*-coordinate, *Tellus, Ser. A*, *51*, 412–430, 1999.

Cavalieri, D. J., P. Gloersen, C. L. Parkinson, J. C. Comiso, and H. J. Zwally, Observed hemispheric asymmetry in global sea ice changes, *Science*, *278*, 1104–1106, 1997.

Chapman, W. L., and J. E. Walsh, Recent variations of sea ice and air temperature in high latitudes, *Bull. Am. Meteorol. Soc.*, *74*, 33–47, 1993.

Comiso, J. C., D. J. Cavalieri, C. L. Parkinson, and P. Gloersen, Passive microwave algorithms for sea ice concentration: A comparison of two techniques, *Remote Sens. Environ.*, *60*, 357–384, 1997.

Danabasoglu, G., and J. C. McWilliams, Sensitivity of the global ocean circulation to parameterizations of mesoscale tracer transports, *J. Clim.*, *8*, 2967–2987, 1995.

de la Mare, W. K., Abrupt mid-twentieth-century decline in Antarctic sea-ice extent from whaling records, *Nature*, *389*, 57–60, 1997.

Deleersnijder, E., and J.-M. Campin, On the computation of the barotropic mode of a free-surface World Ocean model, *Ann. Geophys.*, *13*, 675–688, 1995.

Drinkwater, M. R., and X. Liu, Active and passive microwave determination of the circulation and characteristics of the Weddell and Ross sea ice, in *Proceedings IGARSS'99*, *Hamburg*, *Germany*, *28 June–2 July, 1999*, vol. 1, *99CH36293*, pp. 314–316, Inst. of Electr. and Electron. Eng., New York, 1999.

England, M. H., and A. C. Hirst, Chlorofluorocarbon uptake in a World Ocean model: 2. Sensitivity to surface thermohaline forcing and subsurface mixing parameterizations, *J. Geophys. Res.*, *102*, 15,709–15,731, 1997.

Fichefet, T., and M. A. Morales Maqueda, Sensitivity of a global sea ice model to the treatment of ice thermodynamics and dynamics, *J. Geophys. Res.*, *102*, 12,609–12,646, 1997.

Fichefet, T., and M. A. Morales Maqueda, Modelling the influence of snow accumulation and snow-ice formation on the seasonal cycle of the Antarctic sea-ice cover, *Clim. Dyn.*, *15*, 251–268, 1999.

Fichefet, T., B. Tartinville, and H. Goosse, Sensitivity of the Antarctic sea ice to the thermal conductivity of snow, *Geophys. Res. Lett.*, *27*, 401–404, 2000.

Fischer, H., and P. Lemke, On the required accuracy of atmospheric forcing fields for driving dynamic-thermodynamic sea ice models, in *The Polar Oceans and Their Role in Shaping the Global Environment: The Nansen Centennial Volume*, *Geophys. Monogr. Ser.*, vol. 85, edited by O. M. Johannessen, R. D. Muench, and J. E. Overland, pp. 373–381, AGU, Washington, D. C., 1994.

Folland, C. K., T. R. Karl, J. R. Christy, R. A. Clarke, G. V. Gruza, J. Jouzel, M. E. Mann, J. Oerlemans, M. J. Salinger, and S.-W. Wang, Observed climate variability and change, in *Climate Change 2001: The Scientific Basis: Contribution of Working Group I to the Third Assessment Report of the Intergovernmental Panel on Climate Change*, edited by J. T. Houghton et al., pp. 99–181, Cambridge Univ. Press, New York, 2001.

Gent, P. R., Isopycnal mixing in ocean circulation models, *J. Phys. Oceanogr.*, *20*, 150–155, 1990.

Giles, K. A., and S. W. Laxon, Comparison of satellite-derived sea ice thickness and motion between October 1993 and March 1998 [CD-ROM], *Geophys. Res. Abstr.*, *3*, 2001.

Gloersen, P., W. J. Campbell, D. J. Cavalieri, J. C. Comiso, C. L. Parkinson, and H. J. Zwally, Arctic and Antarctic sea ice, 1978–1987: Satellite passive-microwave observations and analysis, *NASA Spec. Publ.*, *SP-511*, 290 pp., 1992.

Gloersen, P., C. L. Parkinson, D. J. Cavalieri, J. C. Comiso, and H. J. Zwally, Spatial distribution of trends and seasonality in the hemispheric sea ice covers: 1978–1996, *J. Geophys. Res.*, *104*, 20,827–20,835, 1999.

Goosse, H., Modelling the large-scale behaviour of the coupled ocean-sea-ice system, Ph.D. thesis, 231 pp., Fac. des Sci. Appl., Univ. Cath. de Louvain, Louvain-la-Neuve, Belgium, 1997.

Goosse, H., and T. Fichefet, Importance of ice-ocean interactions for the global ocean circulation: A model study, *J. Geophys. Res.*, *104*, 23,337–23,355, 1999.

Goosse, H., E. Deleersnijder, T. Fichefet, and M. England, Sensitivity of a global coupled ocean-sea ice model to the parameterization of vertical mixing, *J. Geophys. Res.*, *104*, 13,681–13,695, 1999.

Goosse, H., J.-M. Campin, and B. Tartinville, The sources of Antarctic Bottom Water in a global ice-ocean model, *Ocean Modell. 3*, pp. 51–65, Hooke Inst. Oxford Univ., Oxford, England, 2001.

Grabs, W., T. De Crouet, and J. Pauler, Freshwater fluxes from continents into the world oceans based on the data of the global runoff data base, *Global Runoff Data Centre Rep. 10*, 228 pp., Fed. Inst. of Hydrol., Koblenz, Germany, 1996.

Harangozo, S. A., Atmospheric meridional circulation impacts on contrasting winter sea ice extent in two years in the Pacific sector of the Southern Ocean, *Tellus, Ser. A*, *49*, 388–400, 1997.

Harder, M., and H. Fischer, Sea ice dynamics in the Weddell Sea simulated with an optimized model, *J. Geophys. Res.*, *104*, 11,151–11,162, 1999.

Harms, S., E. Fahrbach, and V. H. Strass, Sea ice transports in the Weddell Sea, *J. Geophys. Res.*, *106*, 9057–9073, 2001.

Hibler, W. D., III, A dynamic thermodynamic sea ice model, *J. Phys. Oceanogr.*, *9*, 815–846, 1979.

Hibler, W. D., III, and S. F. Ackley, Numerical simulation of the Weddell Sea pack ice, *J. Geophys. Res.*, *88*, 2873–2887, 1983.

Hines, K. M., D. H. Bromwich, and G. J. Marshall, Artificial surface pressure trends in the NCEP–NCAR reanalysis over the Southern Ocean and Antarctica, *J. Clim.*, *13*, 3940–3952, 2000.

Hirst, A. C., and T. J. McDougall, Deep water properties and surface buoyancy flux as simulated by a z-coordinate model including eddy-induced advection, *J. Phys. Oceanogr.*, *26*, 1320–1343, 1996.

Holland, D. M., Explaining the Weddell Polynya—A large ocean eddy shed at Maud Rise, *Science*, *292*, 1697–1700, 2001.

Hurrell, J. W., and H. van Loon, A modulation of the atmospheric annual cycle in the Southern Hemisphere, *Tellus, Ser. A*, *46*, 325–338, 1994.

Jeffries, M. O., and U. Adolphs, Early winter ice and snow thickness distribution, ice structure and development on the western Ross Sea pack ice between the ice edge and the Ross Ice Shelf, *Antarct. Sci.*, *9*, 188–200, 1997.

Jeffries, M. O., R. A. Shaw, K. Morris, A. L. Veazey, and H. R. Krouse, Crystal structure, stable isotopes ($\delta^{18}O$), and development of sea ice in the Ross, Amundsen, and Bellingshausen Seas, Antarctica, *J. Geophys. Res.*, *99*, 985–995, 1994.

Kalnay, E., et al., The NCEP/NCAR 40-year reanalysis project, *Bull. Am. Meteorol. Soc.*, *77*, 437–470, 1996.

Kistler, R, et al., The NCEP–NCAR 50-year reanalysis: Monthly means CD-ROM and documentation, *Bull. Am. Meteorol. Soc.*, *82*, 247–267, 2001.

Lange, M. A., and H. Eicken, The sea ice thickness distribution in the northwestern Weddell Sea, *J. Geophys. Res.*, *96*, 4821–4837, 1991.

Large, W. G., and S. Pond, Open ocean momentum flux measurements in moderate to strong winds, *J. Phys. Oceanogr.*, *11*, 324–336, 1981.

Legutke, S., E. Maier-Reimer, A. Stössel, and A. Hellbach, Ocean-sea ice coupling in a global ocean general circulation model, *Ann. Glaciol.*, *25*, 116–120, 1997.

Levitus, S., Climatological atlas of the World Ocean, *NOAA Prof. Pap. 13*, 173 pp., U.S. Gov. Print. Off., Washington, D. C., 1982.

Markus, T., and D. J. Cavalieri, An enhancement of the NASA Team sea ice algorithm, *IEEE Trans. Geosci. Remote Sens.*, *38*, 1387–1398, 2000.

Marsland, S. J., and J.-O. Wolff, On the sensitivity of the Southern Ocean sea ice to the surface freshwater flux: A model study, *J. Geophys. Res.*, *106*, 2723–2741, 2001.

Maslanik, J., T. Agnew, M. Drinkwater, W. Emery, V. Fowler, R. Kwok, and A. Liu, Summary of ice-motion mapping using passive microwave data, *NSIDC Spec. Publ. 8.*, 25 pp., Natl. Snow and Ice Data Cent., Univ. of Colo., Boulder, Colo., 1998.

Meehl, G. A., A reexamination of the mechanism of the semiannual oscillation in the Southern Hemisphere, *J. Clim.*, *4*, 911–926, 1991.

Meehl, G. A., J. W. Hurrell, and H. van Loon, A modulation of the mechanism of the semiannual oscillation in the Southern Hemisphere, *Tellus, Ser. A*, *50*, 442–450, 1998.

Mellor, G. L., and T. Yamada, Development of a turbulence closure model for geophysical fluid problems, *Rev. Geophys.*, *20*, 851–875, 1982.

National Snow and Ice Data Center, Bootstrap sea ice concentrations from Nimbus 7 SMMR and DMSP SSM/I, NSIDC Distrib. Active Arch. Cent., Univ. of Colo., Boulder, 1999. (Digital data available from nsidc@kryos.colorado.edu)

Steffen, K., J. Key, D. J. Cavalieri, J. Comiso, P. Gloersen, K. St. Germain, and I. Rubinstein, The estimation of geophysical parameters using passive microwave algorithms, in *Microwave Remote Sensing of Sea Ice*, *Geophys. Monogr. Ser.*, vol. 68, edited by F. D. Carsey, pp. 201–231, AGU, Washington, D.C., 1992.

Stössel, A., Sensitivity of the Southern Ocean sea-ice simulations to different atmospheric forcing algorithms, *Tellus, Ser. A*, *44*, 395–413, 1992.

Stössel, A., S. J. Kim, and S. S. Drijfout, The impact of Southern Ocean sea ice in a global ocean model, *J. Phys. Oceanogr.*, *28*, 1999–2018, 1998.

Strass, V. H., and E. Fahrbach, Temporal and regional variation of sea ice draft and coverage in the Weddell Sea obtained from upward looking sonars, in *Antarctic Sea Ice: Physical Processes, Interactions and Variability*, *Antarct. Res. Ser.*, vol. 74, edited by M. O. Jeffries, pp. 123–139, AGU, Washington, D. C., 1998.

Tartinville, B., J.-M. Campin, T. Fichefet, and H. Goosse, Realistic representation of the freshwater flux in an ice-ocean general circulation model, *Ocean Modell.*, *3*, 95–108, 2001.

Tartinville, B., A. Cavanié, R. Ezraty, and T. Fichefet, Artic multiyear ice coverage: A model study, *Inst. d'Astron. et de Géophys. Georges Lemaître Sci. Rep. 2002/1*, 53 pp., Univ. Cath. de Louvain, Louvain-la-Neuve, Belgium, 2002.

Timmermann, R., A. Beckmann, and H. H. Hellmer, Simulations of ice-ocean dynamics in the Weddell Sea: 1. Model configuration and validation, *J. Geophys. Res.*, *108*, 3024, doi:10.1029/2000JC000741, 2002a.

Timmermann, R., H. H. Hellmer, and A. Beckmann, Simulations of ice-ocean dynamics in the Weddell Sea: 2. Interannual variability 1985–1993, *J. Geophys. Res.*, *108*, 3025, doi:10.1029/2000JC000742, 2002b.

Trenberth, K. E., J. G. Olson, and W. G. Large, A global ocean wind stress climatology based on the ECMWF analyses, *NCAR/TN-338+STR*, 93 pp., Natl. Cent. for Atmos. Res., Boulder, Colo., 1989.

Van den Broecke, M. R., The semiannual oscillation and Antarctic climate: 2. Recent changes, *Antarct. Sci.*, *10*, 184–191, 1998.

Van den Broecke, M. R., The semiannual oscillation and Antarctic climate: 4. A note on sea ice cover in the Amundsen and Bellingshausen Seas, *Int. J. Climatol.*, *20*, 455–462, 2000a.

Van den Broecke, M. R., The semiannual oscillation and Antarctic climate: 5. Impact on the annual temperature cycle as derived from the NCEP/NCAR re-analysis, *Clim. Dyn.*, *16*, 366–377, 2000b.

Van den Broecke, M. R., On the interpretation of Antarctic temperature trends, *J. Clim.*, *13*, 3885–3889, 2000c.

van Loon, H., The half-yearly oscillations in the middle and high southern latitudes and the coreless winter, *J. Atmos. Sci.*, *24*, 472–486, 1967.

van Loon, H., J. W. Kidson, and A. B. Mullan, Decadal variation of the annual cycle in the Australian dataset, *J. Clim.*, *6*, 1227–1231, 1993.

Wadhams, P., Sea ice thickness changes and their relation to climate, in *The Polar Oceans and Their Role in Shaping the Global Environment: The Nansen Centennial Volume*, *Geophys. Monogr. Ser.*, vol. 85, edited by O. M. Johannessen, R. D. Muench, and J. E. Overland, pp. 337–362, AGU, Washington, D. C., 1994.

Watkins, A. B., and I. Simmonds, Current trends in Antarctic sea ice: The 1990s impact on a short climatology, *J. Clim.*, *13*, 4441–4451, 2000.

Weatherly, J. W., J. E. Walsh, and H. J. Zwally, Antarctic sea ice variations and seasonal air temperature relationships, *J. Geophys. Res.*, *96*, 15,119–15,130, 1991.

White, W. B., and R. G. Peterson, An Antarctic circumpolar wave in surface pressure, wind, temperature and sea-ice extent, *Nature*, *380*, 699–702, 1996.

Windmüller, M., Untersuchung von atmosphärischen reanalysedaten im Weddellmeer und anwendung auf ein dynamisch thermodynamisches meereismodell, M.S. thesis, 65 pp., Inst. für Meereskunde, Christian-Albrechts-Univ. zu Kiel, Kiel, Germany, 1997.

Worby, A. P., M. O. Jeffries, W. F. Weeks, K. Morris, and R. Jaña, The thickness distribution of sea ice and snow cover during late winter in the Bellingshausen and Amundsen Seas, Antarctica, *J. Geophys. Res.*, *101*, 28,441–28,455, 1996.

Worby, A. P., R. A. Massom, I. Allison, V. I. Lytle, and P. Heil, East Antarctic sea ice: A review of its structure, properties and drift, in *Antarctic Sea Ice: Physical Processes, Interactions and Variability*, *Antarct. Res. Ser.*, vol. 74, edited by M. O. Jeffries, pp. 41–67, AGU, Washington, D.C., 1998.

World Climate Research Programme, Climate and Cryosphere (CliC) project, Science and co-ordination plan, version 1, *WCRP-114*, *WMO/TD No. 1053*, edited by I. Allison, R. G. Barry, and B. E. Goodison, 75 pp., World Meteorol. Org., Geneva, 2001.

Xie, P., and P. A. Arkin, Analyses of global monthly precipitation using gauge observations, satellite estimates and numerical model predictions, *J. Clim.*, *9*, 840–858, 1996.

Zwally, H. J., J. C. Comiso, C. L. Parkinson, W. J. Campbell, F. D. Carsey, and P. Gloersen, Antarctic sea ice, 1973–1976: Satellite passive-microwave observations, *NASA Spec. Publ.*, *SP-459*, 206 pp., 1983.

T. Fichefet, H. Goosse, and B. Tartinville, Institut d'Astronomie et de Géophysique Georges Lemaître, Université Catholique de Louvain, B-1348 Louvain-la-Neuve, Belgium. (fichefet@astr.ucl.ac.be; hgs@astr.ucl.ac.be; tartin@numeca.be)